PERGAMON

Computerized Medical Imaging and Graphics 25 (2001) 465–476

Computerized Medical Imaging and Graphics

www.elsevier.com/locate/compmedimag

Orthogonal subspace projection-based approaches to classification of MR image sequences

C.-M. Wang[a], S.-C. Yang[a], P.-C. Chung[a], C.-I Chang[b,*], C.-S. Lo[a], C.-C. Chen[c], C.-W. Yang[d], C.-H. Wen[d]

[a]*Department of Electrical Engineering, National Cheng Kung University, 1 University Road, Tainan, Taiwan*
[b]*Remote Sensing Signal and Image Processing Laboratory, Department of Computer Science and Electrical Engineering, University of Maryland, Baltimore County, Baltimore, MD 21250, USA*
[c]*Department of Radiology, Taichung Veterans General Hospital, Taichung 407, Taiwan*
[d]*Computer Center, Taichung Veterans General Hospital, Taichung 407, Taiwan*

Received 24 September 1999; accepted 4 April 2001

Abstract

Orthogonal subspace projection (OSP) approach has shown success in hyperspectral image classification. Recently, the feasibility of applying OSP to multispectral image classification was also demonstrated via SPOT (Satellite Pour 1'Observation de la Terra) and Landsat (Land Satellite) images. Since an MR (magnetic resonance) image sequence is also acquired by multiple spectral channels (bands), this paper presents a new application of OSP in MR image classification. The idea is to model an MR image pixel in the sequence as a linear mixture of substances (such as white matter, gray matter, cerebral spinal fluid) of interest from which each of these substances can be classified by a specific subspace projection operator followed by a desired matched filter. The experimental results show that OSP provides a promising alternative to existing MR image classification techniques.

Keywords: Classification; Generalized orthogonal subspace projection (GOSP); Orthogonal subspace projection; Magnetic resonance imaging (MRI)

1. Introduction

Magnetic resonance imaging (MRI) has become a useful modality because it provides unparallel capability of revealing soft tissue characterization as well as 3-D visualization. It produces a sequence of multiple spectral images of tissues with a variety of contrasts using three magnetic resonance parameters, spin-lattice (T1), spin-spin (T2) and dual echo-echo proton density (PD). One potential application of MRI in clinical practice is the brain parenchyma classification and segmentation of normal and pathological tissue. It is the first step to address a wide range of clinical problems. Using the volume, shapes and region distribution of the brain tissue, one can find the abnormalities that are commonly related to conditions of heterotopia, lissencephaly, brain atrophy, and cerebral infarction. Over the past years many computer-assisted methods have been reported in the literature [1–11] such as neural networks [5–9], hybrid methods [10], knowledge-based techniques [11], etc. For example, neural networks have demonstrated their superior performance in segmentation of brain tissue to classical maximum likelihood methods. Hybrid methods have shown a promise by combining imaging processing and model-based techniques in segmentation [10]. Knowledge-based techniques allow one to make more intelligent classification and segmentation decisions [11]. In addition, a series of papers based on an eigenimage approach to MR image classification were reported by a leading group in Henry Ford Hospital, Michigan [12–16]. More recently, a Euclidean distance-based discriminant analysis approach was developed by Soltanian-Zadeh et al. [17] for MRI feature extraction. In this paper, we present a new approach to MRI classification that is based on spectral feature correlation among an MR image sequence. It is derived from the concept of Orthogonal Subspace Projection (OSP) which was originally developed for hyperspectral image classification [18]. Nonetheless, it owes its originality to the idea developed in [19,20]. Most interestingly, it was also shown in [21] that Soltanian-Zadeh et al.'s optimal linear transformation [17] was equivalent to the OSP approach provided the target vectors were constrained to be orthogonal.

The OSP approach which can be also found in [22] has

* Corresponding author. Tel.: +1-410-455-3502; fax: +1-410-455-3969.
E-mail address: cchang@umbc.edu (C.-I Chang).

0895-6111/01/$ - see front matter
PII: S0895-6111(01)00015-5

shown success in AVIRIS (Airborne Visible/InfraRed Imaging Spectrometer) and HYDICE (HYperspectral Digital Imagery Collection Experiment) data exploitation [23,24]. It assumes that a hyperspectral image contains a complete knowledge of object signatures present in the image scene and each pixel is then modeled as a linear mixture of these signatures. By taking advantage of this linear mixture model the assumed objects can be extracted by a specific subspace projection operator followed by a desired matched filter. Since an MR image sequence is multispectral images, they can be also viewed as remotely sensed images. With this interpretation, OSP provides a feasible approach to classification of an MR image sequence.

However, it has also shown in [25] that in order for the OSP approach to be effective, the data dimensionality must be sufficiently large to accommodate orthogonal subspace projection. In particular, the number of signatures to be classified cannot be greater than the number of spectral channels (bands) to be used to acquire the data. More precisely, if we want to classify objects effectively using OSP, each object requires a separate dimension for orthogonal projection. This can be explained by a well-known Pigeon-hole principle [26]. That is, if there are m pigeons flying into $n < m$ holes, then there exists at least one hole that accommodates two or more pigeons. In other words, if there is a dimension used to accommodate two or more objects, the Pigeon-hole principle simply says that it is impossible to discriminate these objects using a single dimension through orthogonal projection. This constraint, referred to as Band Number Constraint (BNC) was discussed in [27] and limits the OSP application only to hyperspectral images where there are hundreds of spectral channels (bands) used for data acquisition and the number of object signatures are generally much less than the number of spectral channels.

In order to apply OSP to multispectral images, the BNC must be relaxed. A general approach is to reduce the number of objects to be classified to accommodate the insufficient data dimensionality. However, this may not be appropriate for some multispectral images. For example, it showed in [27] that SPOT (Satellite Pour 1'Observation de la Terra) images had difficulty with using 3 bands to classify four objects via OSP. As an alternative, an approach, referred to as Generalized OSP (GOSP) was proposed in [28] where it expanded original data dimensionality without compromising the number of objects to be classified. Instead of reducing the number of objects to be classified, GOSP increases the number of images by creating new band images so that the total number of band images to be used can be greater than the number of objects. These extra images are produced nonlinearly and can provide very useful nonlinear information to improve classification performance. By taking advantage of these newly generated nonlinear-correlated images the BNC can be relaxed to make OSP applicable to multispectral image classification, thus can be also applicable to MR image classification. A sequence of brain MR images is used for experiments to demonstrate the performance of OSP and GOSP in MR image classification. As expected, GOSP performs well and can be used for classification of cerebral tissues.

One of most advantages of OSP-based approaches over the traditional classification techniques is that the former is the mixed pixel classification while the latter is the pure-pixel classification. More specifically, mixed pixel classification used a linear spectral mixture model to describe a mixture of substances present in a pixel. It then estimates and uses the abundance fractions of these substances as a base to classify each of these substances. As a result, the images generated by the mixed pixel classification are generally gray scale fractional images of these substances with gray level values determined by the estimated abundance fractions. Comparing to the mixed pixel classification, the pure pixel classification performs a class-membership assignment on a pure pixel basis. In this case, a pixel is determined by a binary decision, either in one class or not. As will be shown in the experiments, the mixed pixel classification allows one to display classification results in color for visualization from which a mixing color indicates a mixture of different substances, a task that cannot be achieved by the pure pixel classification.

The remainder of this paper is organized as follows. Section 2 formulates classification of an MR image sequence as a linear mixing problem. Section 3 describes the OSP approach described in [18,23]. Section 4 describes the GOSP approach developed in [28]. Section 5 conducts a set of experiments to evaluate the performance of OSP and GOSP in MR classification. Section 6 concludes some comments.

2. Linear spectral mixture model

Linear spectral unmixing is a widely used method in remote sensing community to classify and quantify multi-component constituents [29–31]. It views a multi/hyperspectral image as an image cube where each pixel is considered to be a column vector and is modeled as a linear spectral mixture of substances resident in the pixel. More precisely, assume that there are p spectrally distinct substances $\{\mathbf{m}_1, \mathbf{m}_2, \ldots, \mathbf{m}_p\}$ in the image and $\mathbf{r}$ is an image pixel vector represented by an $l \times 1$ column vector where l is the number of spectral bands. Let $\mathbf{M}$ be an $l \times p$ signature matrix, denoted by $[\mathbf{s}_1\ \mathbf{s}_2\ \ldots\ \mathbf{s}_p]$ where $\mathbf{s}_j$ is an $l \times 1$ column vector represented by the spectral signature of the j-th substance $\mathbf{m}_j$ in the pixel vector $\mathbf{r}$. It further assumes that α is a $p \times 1$ abundance column vector associated with $\mathbf{M}$ given by $\alpha = (\alpha_1\ \alpha_2\ \ldots\ \alpha_p)^T$ where T is the transpose, α_j denotes the fraction of the j-th signature $\mathbf{s}_j$ present in the pixel vector $\mathbf{r}$. Then a linear spectral mixture model used to

describe $\mathbf{r}$ is given by

$$\mathbf{r} = \mathbf{M}\alpha + \mathbf{n}. \tag{1}$$

The $\mathbf{n}$ in Eq. (1) is an $l \times 1$ column vector and can be interpreted as either additive noise or measurement error. The linear spectral unmixing is to develop a method that finds or unmixes the abundance vector α from the pixel vector $\mathbf{r}$ through Eq. (1). By viewing an MR image sequence as a multispectral image we can stack T1-weighted, T2-weighted and PD-weighted images one atop another as an image cube where each pixel in the cube is actually a pixel vector. The dimensionality of the pixel vector, l is determined by the MR image sequence used to form the cube. In this case, Eq. (1) models each pixel vector in the cube as a linear mixture of tissue substances resident in the MR images. Specifically, $\mathbf{r}$ is a pixel vector of the image cube formed by an MR image sequence. $\mathbf{M} = [\mathbf{s}_1\ \mathbf{s}_2 \ldots \mathbf{s}_p]$ is a signature matrix made up of the spectral signatures $\{\mathbf{s}_1, \mathbf{s}_2, \ldots, \mathbf{s}_p\}$ of tissue substances $\{\mathbf{m}_1, \mathbf{m}_2, \ldots, \mathbf{m}_p\}$ in the MR image cube such as white matter, gray matter, cerebral spinal fluid, etc. The associated abundance vector α represents the abundance fractions of these p spectral signatures $\{\mathbf{s}_1, \mathbf{s}_2, \ldots, \mathbf{s}_p\}$ present in the pixel vector $\mathbf{r}$. In light of this model formulation, MR image classification can be solved by unmixing the abundance vector α in a mixed pixel represented by Eq. (1).

3. Orthogonal subspace projection-based approaches

Many unmixing methods have been proposed to solve Eq. (1) in the past [31]. Of particular interest is the OSP approach that has been successfully applied to hyperspectral images [18,22–24].

3.1. Orthogonal subspace projection (OSP)

The idea of OSP is to divide the p substances into two classes, desired substance class and undesired substance class. Without loss of generality we assume that the desired substance class contains only one single substance and undesired substance class consists of the remaining $p - 1$ substances, denoted by $\mathbf{U}$. Then we can rewrite Eq. (1) as

$$\mathbf{r} = \mathbf{d}\alpha_p + \mathbf{U}\gamma + \mathbf{n} \tag{2}$$

where $\mathbf{d} = \mathbf{s}_p$ is the desired substance, $\mathbf{U} = [\mathbf{s}_1\ \mathbf{s}_2 \ldots \mathbf{s}_{p-1}]$ is the matrix consisting of undesired substances, α_p is the abundance fraction of the desired spectral signature $\mathbf{d}$ and $\gamma = (\alpha_1\ \alpha_2 \ldots \alpha_{p-1})^T$ is the abundance vector representing fractions of the undesired spectral signatures $\{\mathbf{s}_1, \mathbf{s}_2, \ldots, \mathbf{s}_{p-1}\}$.

Since the desired signature $\mathbf{d}$ is separated from the undesired signatures $\{\mathbf{s}_1, \mathbf{s}_2, \ldots, \mathbf{s}_{p-1}\}$ in Eq. (2), we can design a subspace projection operator to eliminate $\{\mathbf{s}_1, \mathbf{s}_2, \ldots, \mathbf{s}_{p-1}\}$ before extracting $\mathbf{d}$. One such a projector is the least squares operator $P_{\mathbf{U}}^{\perp}$ given by

$$P_{\mathbf{U}}^{\perp} = \mathbf{I} - \mathbf{U}\mathbf{U}^{\#} \tag{3}$$

where $\mathbf{U}^{\#} = (\mathbf{U}^T\mathbf{U})^{-1}\mathbf{U}^T$ is the pseudo-inverse of $\mathbf{U}$ and the notation $^{\perp}_{\mathbf{U}}$ in $P_{\mathbf{U}}^{\perp}$ indicates that the projector maps the observed pixel $\mathbf{r}$ into the space $\langle \mathbf{U} \rangle^{\perp}$, the orthogonal complement of $\mathbf{U}$. Premultiplying Eq. (2) by $P_{\mathbf{U}}^{\perp}$ yields

$$P_{\mathbf{U}}^{\perp}\mathbf{r} = P_{\mathbf{U}}^{\perp}\mathbf{d}\alpha_p + P_{\mathbf{U}}^{\perp}\mathbf{U}\gamma + P_{\mathbf{U}}^{\perp}\mathbf{n} = \mathbf{d}\alpha_p + P_{\mathbf{U}}^{\perp}\mathbf{n} \tag{4}$$

where the undesired substances $\{\mathbf{s}_1, \mathbf{s}_2, \ldots, \mathbf{s}_{p-1}\}$ have been eliminated by $P_{\mathbf{U}}^{\perp}$ and the original noise is also suppressed to $P_{\mathbf{U}}^{\perp}\mathbf{n}$ by $P_{\mathbf{U}}^{\perp}$. As a result, Eq. (4) represents a standard signal detection model. If the optimal criterion for the signal detection specified by (4) is chosen to maximize the Signal-to-Noise Ratio (*SNR*) defined by

$$SNR = \frac{(\mathbf{x}^T P_{\mathbf{U}}^{\perp}\mathbf{d})\ \alpha_p (d^T P_{\mathbf{U}}^{\perp}\mathbf{x})}{(\mathbf{x}^T P_{\mathbf{U}}^{\perp})\ E[\mathbf{n}\mathbf{n}^T](P_{\mathbf{U}}^{\perp}\mathbf{x})} \qquad \text{over } x. \tag{5}$$

The maximum *SNR* of Eq. (5) can be achieved by a matched filter, denoted by $MF_{\mathbf{d}}$ with $\mathbf{d}$ chosen to be the desired matched signal. Namely, $MF_{\mathbf{d}}$ is an operator given by

$$MF_{\mathbf{d}}(\mathbf{x}) = \mathbf{d}^T\mathbf{x} \text{ for any pixel vector } \mathbf{x} \tag{6}$$

Based on Eqs. (4) and (5), a mixed pixel classification can be carried out by a two-stage process, i.e. an undesired signature annihilator, $P_{\mathbf{U}}^{\perp}$ followed by a matched filter, $MF_{\mathbf{d}}$. In other words, if we want to classify a desired signature $\mathbf{d}$ in a mixed pixel described by Eq. (1), we first apply $P_{\mathbf{U}}^{\perp}$ to Eq. (2) to eliminate $\mathbf{U}$, then use the matched filter $MF_{\mathbf{d}}$ to extract $\mathbf{d}$ from Eq. (4). The operator $P_{\mathbf{U}}^{\perp}$ coupling with $MF_{\mathbf{d}}$ is called an orthogonal subspace classifier, P_{OSP} derived in [18] and given by

$$P_{\mathrm{OSP}} = MF_{\mathbf{d}}P_{\mathbf{U}}^{\perp} = \mathbf{d}^T P_{\mathbf{U}}^{\perp} \tag{7}$$

3.2. A posteriori OSP

When OSP used Eq. (1) to derive Eq. (7), it assumed a complete knowledge of the linear mixture model except the noise $\mathbf{n}$. However, this is not true in many practical applications, specifically, the signature abundance vector α which is generally not known in practice. In [23] the OSP was extended to a posteriori OSP to improve the OSP by including a posteriori information in the OSP-generated classifier, P_{OSP} specified by Eq. (7). Three a posteriori OSP-based classifiers were derived in [23], referred to as Signature Subspace Classifier (SSC), Target Subspace Classifier (TSC) and Oblique Subspace Classifier (OBC). Since SSC and OBC are of practical interest and are applicable to MR image classification, they will be discussed below.

3.2.1. Signature Subspace Classifier (SSC)

In order to take advantage of a posteriori information, the least squares error approach was used in [23] to derive the estimate of the unknown abundance vector,

$\hat{\alpha}_{\mathrm{LS}}(\mathbf{r})$ given by

$$\hat{\alpha}_{\mathrm{LS}}(\mathbf{r}) = (\mathbf{M}^T\mathbf{M})^{-1}\mathbf{M}^T\mathbf{r} \tag{8}$$

where the pixel vector $\mathbf{r}$ is included in $\hat{\alpha}_{\mathrm{LS}}(\mathbf{r})$ to reflect the dependency of the estimate on the a posteriori information obtained from $\mathbf{r}$. From Eq. (8) we can define a signature subspace projector $P_{\mathbf{M}}$ by

$$P_{\mathbf{M}} = \mathbf{M}(\mathbf{M}^T\mathbf{M})^{-1}\mathbf{M}^T \tag{9}$$

which yields $P_{\mathbf{M}}\mathbf{M} = \mathbf{M}$. Using Eq. (9), the a posteriori OSP-based SSC, P_{SSC} can be obtained by

$$P_{\mathrm{SSC}} = \mathbf{d}^T P_{\mathbf{U}}^{\perp} P_{\mathbf{M}} = P_{\mathrm{OSP}} P_{\mathbf{M}} \tag{10}$$

It should be noted that the difference between P_{OSP} and P_{SSC} is the inclusion of $P_{\mathbf{M}}$ in Eq. (10) which projects the pixel vector $\mathbf{r}$ into the signature subspace $\langle\mathbf{M}\rangle$ as well as suppresses noise by operating $P_{\mathbf{M}}$ on $\mathbf{r}$

$$P_{\mathbf{M}}\mathbf{r} = P_{\mathbf{M}}\mathbf{M}\mathbf{r} = \mathbf{M}\hat{\alpha}_{\mathrm{LS}}(\mathbf{r}) \tag{11}$$

3.2.2. Oblique Subspace Classifier (OBC)

Unlike SSC, OBC is not an orthogonal projector. It utilizes an oblique operator which projects the desired signature $\mathbf{d}$ into its range space while mapping all the undesired signatures in $\mathbf{U}$ into its null space. In particular, let $E_{\mathbf{XY}}$ be a projector with its range and null spaces specified by X and Y respectively. The OBC can be obtained by an operator, P_{OBC} which implements an oblique projector $E_{\mathbf{dU}}$ defined by Eq. (13) followed by the matched filter $MF_{\mathbf{d}}$ given by Eq. (6). More precisely, P_{OBC} is given by

$$P_{\mathrm{OBC}} = \frac{\mathbf{d}^T E_{\mathbf{dU}}}{\mathbf{d}^T\mathbf{d}} \tag{12}$$

where

$$E_{\mathbf{dU}} = \mathbf{d}(\mathbf{d}^T P_{\mathbf{U}}^{\perp}\mathbf{d})^{-1}\mathbf{d}^T P_{\mathbf{U}}^{\perp} \tag{13}$$

and $E_{\mathbf{dU}}\mathbf{d} = \mathbf{d}$, $E_{\mathbf{dU}}\mathbf{U} = 0$.

It was further shown in [23] that P_{OBC} differs from P_{OSP} by only a constant $(\mathbf{d}^T P_{\mathbf{U}}^{\perp}\mathbf{d})^{-1}$, i.e.

$$P_{\mathrm{OBC}} = \frac{\mathbf{d}^T E_{\mathbf{dU}}}{\mathbf{d}^T\mathbf{d}} = \frac{\mathbf{d}^T P_{\mathbf{U}}^{\perp}}{(\mathbf{d}^T P_{\mathbf{U}}^{\perp}\mathbf{d})} = \frac{P_{\mathrm{OSP}}}{(\mathbf{d}^T P_{\mathbf{U}}^{\perp}\mathbf{d})} \tag{14}$$

More importantly, it also showed in [23,32,33] that if the additive noise in Eq. (1) is Gaussian, P_{OBC} is actually the maximum likelihood classifier (MLC). Because of that OBC can be viewed as a generalized version of MLC.

4. Generalized orthogonal subspace projection (GOSP)

The success of OSP-based classifiers in hyperspectral image classification lies in the fact that the projector $P_{\mathbf{U}}^{\perp}$ described by Eq. (3) rejects undesired signatures in $\mathbf{U}$ prior to the matched filter $MF_{\mathbf{d}}$ given by Eq. (6). In order that $P_{\mathbf{U}}^{\perp}$ can effectively eliminate the undesired signatures, the data dimensionality, l must be greater than $p-1$, the dimensionality of $\langle\mathbf{U}\rangle$. Otherwise, some undesired signatures will be mixed into the space $\langle\mathbf{U}\rangle^{\perp}$. Such constraint imposed by the Pigeon-hole principle is referred to as band number constraint (BNC). So, when the BNC violates, this unwanted mixing distorts $\mathbf{d}$ and further results in poor classification. To alleviate this problem, either the dimensionality of $\langle\mathbf{U}\rangle$ must be reduced to satisfy the BNC or the data dimensionality must be increased to meet the BNC. The former case can be done by eliminating unwanted signatures so that the data dimensionality can be reduced before the classification takes place. One such an approach was reported in [27] where some undesired signatures were considered to be interferers and were eliminated from the undesired signatures space $\langle\mathbf{U}\rangle$ to reduce the dimensionality of $\langle\mathbf{U}\rangle$. However, under this circumstance, we need to know which signatures in $\mathbf{U}$ are interferers with respect to the desired signature $\mathbf{d}$ to achieve an optimal selection.

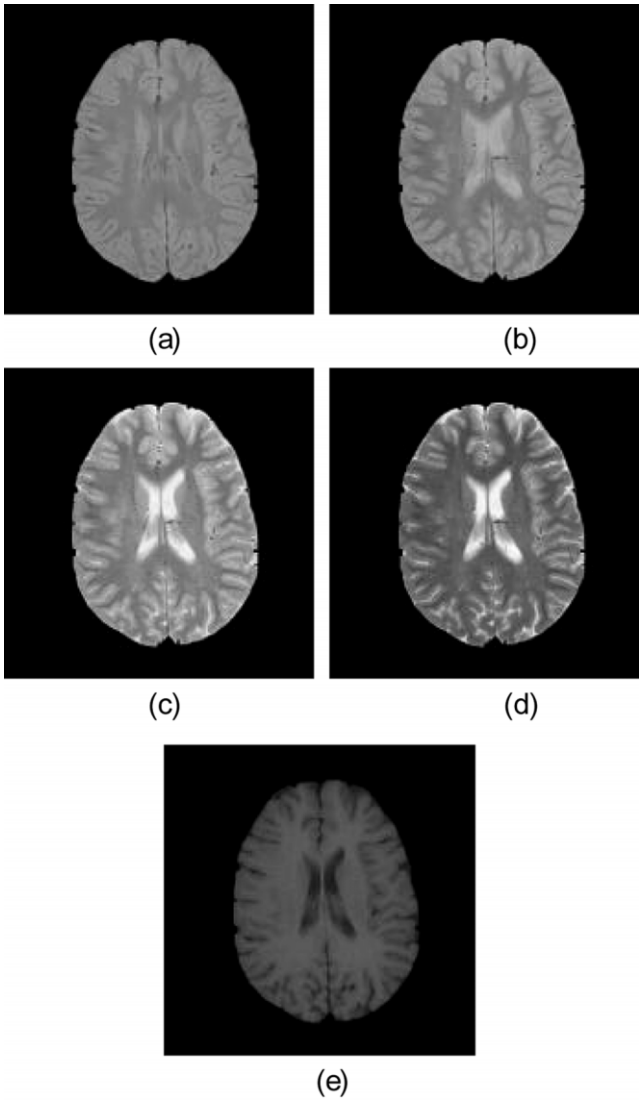

Fig. 1. Five Band MR brain images.

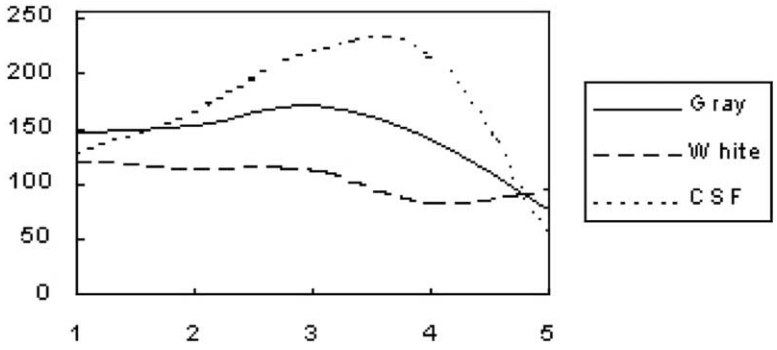

Fig. 2. Spectra of WM, GM and CSF.

In order to do so, we ought to exhaust all possible combinations where each combination must be examined to determine which is the best case for the optimal performance. For instance, if $l \leq p-1$, there are

$$\binom{p-1}{l-1}$$

combinations to remove $p-l$ undesired signatures from $\mathbf{U}$. It is obviously not practical if $p-1$ is much greater than l. As an alternative to reduction of dimensionality of $\langle \mathbf{U} \rangle$, we choose to increase the data dimensionality rather than to reduce the number of signatures from p to l so that there is no need to determine which signatures in $\mathbf{U}$ must be eliminated.

4.1. Dimensionality Expansion (DE)

To expand data dimensionality a Generalized OSP (GOSP) approach was previously developed in [28]. The idea proposed in GOSP arises in the fact that a second-order random process is generally specified by its first-order and second-order statistics. If we view the original band images as the first-order images. We can generate a set of second-order statistics band images by capturing correlations between band images. These correlated images provide useful second-order statistics information about band images which is missing in the set of the original band images. The desired second-order statistics including auto-correlation, cross-correlation and nonlinear correlations now can be used to create

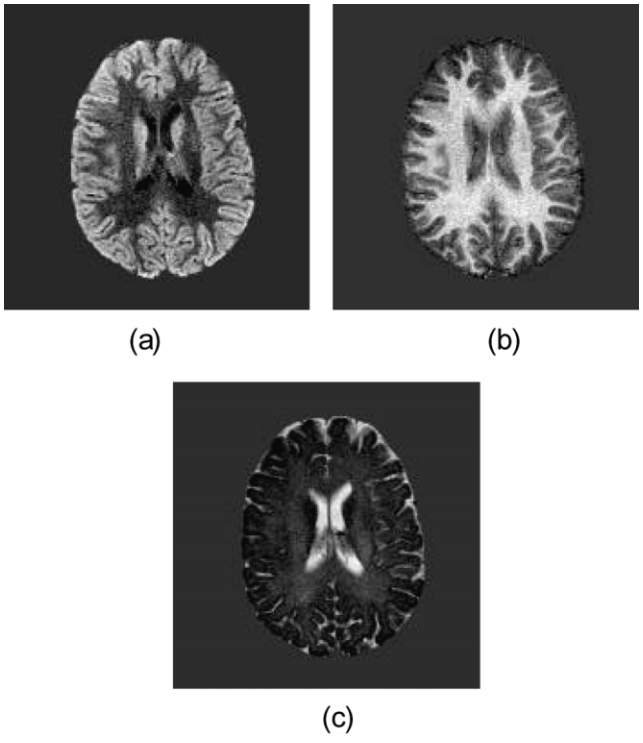

Fig. 3. Classification results of OSP.

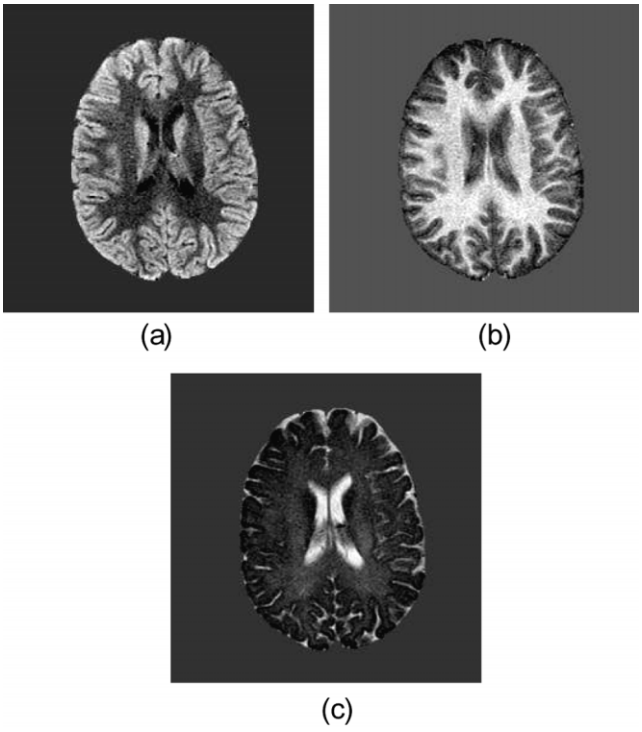

Fig. 4. Classification results of SSC.

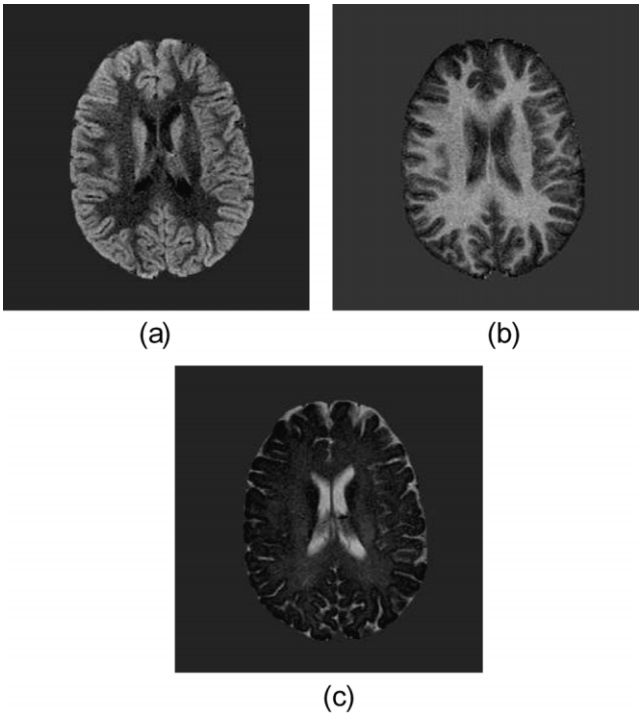

Fig. 5. Classification results of OBC.

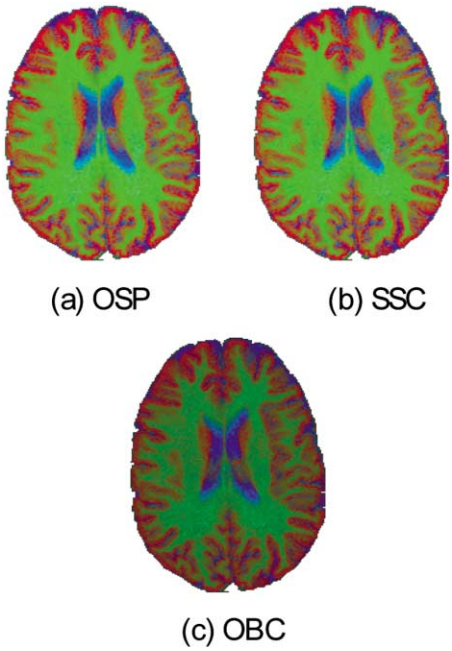

Fig. 6. RGB-colored classification results for OSP, SSC and OBC.

nonlinearly correlated images between band images. The concept of producing second-order correlated band images coincides that used to generate covariance function for a random process.

Let $\{B_i\}_{i=1}^{l}$ be the set of an MR image sequence. The first set of second order-statistics band images generated are based on auto-correlation. They are constructed by multiplying each individual band image itself, i.e. $\{B_i^2\}_{i=1}^{l}$. A second set of second order-statistics band images are made up of all cross-correlated band images which are produced by correlating any arbitrary two different band images, i.e. $\{B_iB_j\}_{i,j=1,i\neq j}^{l}$. Adding these two sets of second order-statistics band images to $\{B_i\}_{i=1}^{l}$ produces a total of

$$l + l + \binom{l}{2} = \frac{l^2 + 3l}{2}$$

band images. In case that more images are needed, nonlinear functions may be used to generate so called nonlinear correlated band images. For example, we may use the square-root or logarithm, i.e. $\{\sqrt{B_i}\}_{i=1}^{l}$ or $\{\log B_i\}_{i=1}^{l}$ to stretch out lower gray level values. In the following, we describe several

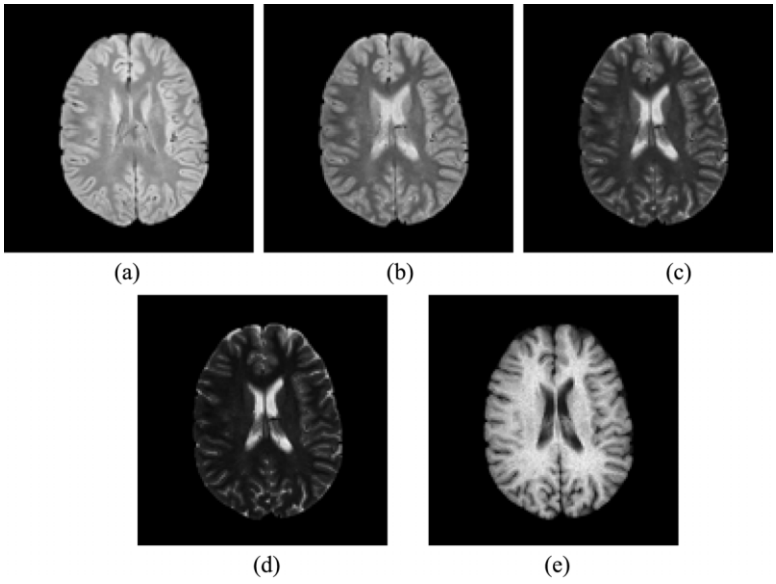

Fig. 7. New images generated by auto-correlation.

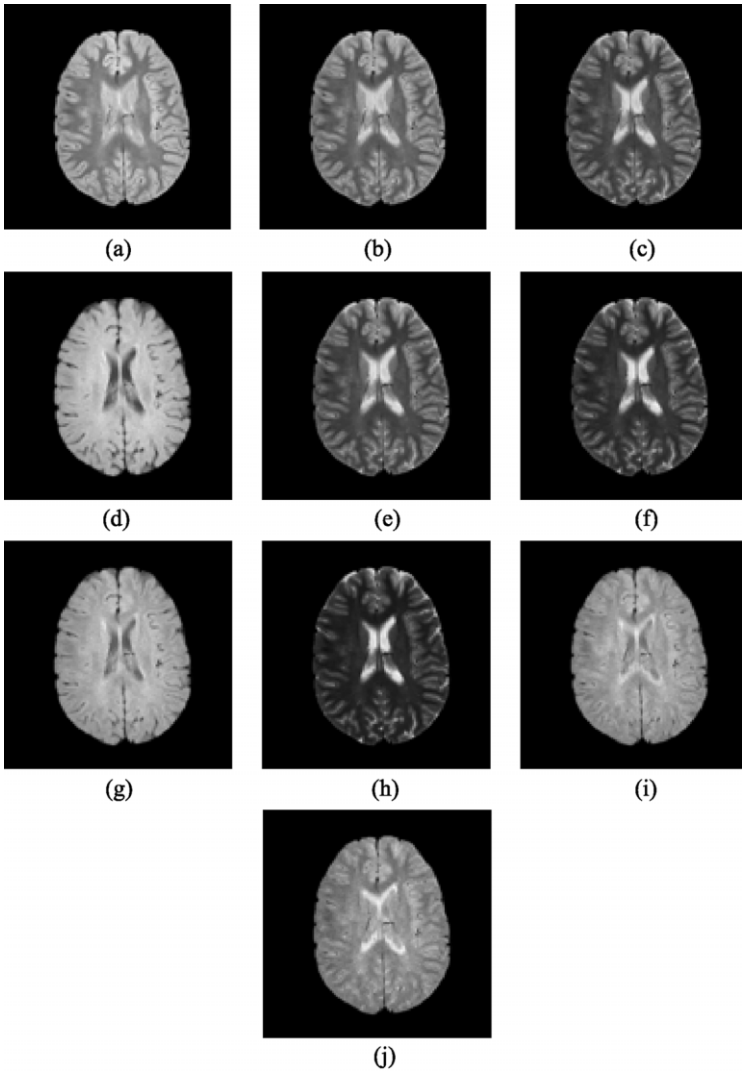

Fig. 8. New images generated by cross-correlation.

ways to generate second-order correlated and other nonlinear correlated band images.

1. First-order band image: $\{B_i\}_{i=1}^{l}$ = set of original band images.
2. Second-order correlated band images:
   2.1. $\{B_i^2\}_{i=1}^{l}$ = set of auto-correlated band images;
   2.2. $\{B_iB_j\}_{i,j=1,i\neq j}^{l}$ = set of cross-correlated band images.
3. Nonlinear correlated band images:
   3.1. $\{\sqrt{B_i}\}_{i=1}^{l}$ = set of band images stretched out by the square-root;
   3.2. $\{\log B_i\}_{i=1}^{l}$ = set of band images stretched out by the logarithmic function.

It should be noted that all the images generated as above are produced nonlinearly. These images are expected to offer useful information for classification because the classifier to be used for object detection and classification is linear and linearly generated band images will not provide extra new information to help the classifier improve performance.

4.2. GOSP algorithm

Since an MR image sequence contains only few images, the data dimensionality is usually not sufficient for orthogonal projection with respect to signatures of interest in the image sequence. As a result, a data dimensionality expansion is necessary for OSP to be effective. In what follows, we describe the detailed implementation of GOSP.

1. Apply DE to expand original image data:
   1.1. generate $\{B_i^2\}_{i=1}^{l}$ = set of auto-correlated band images;

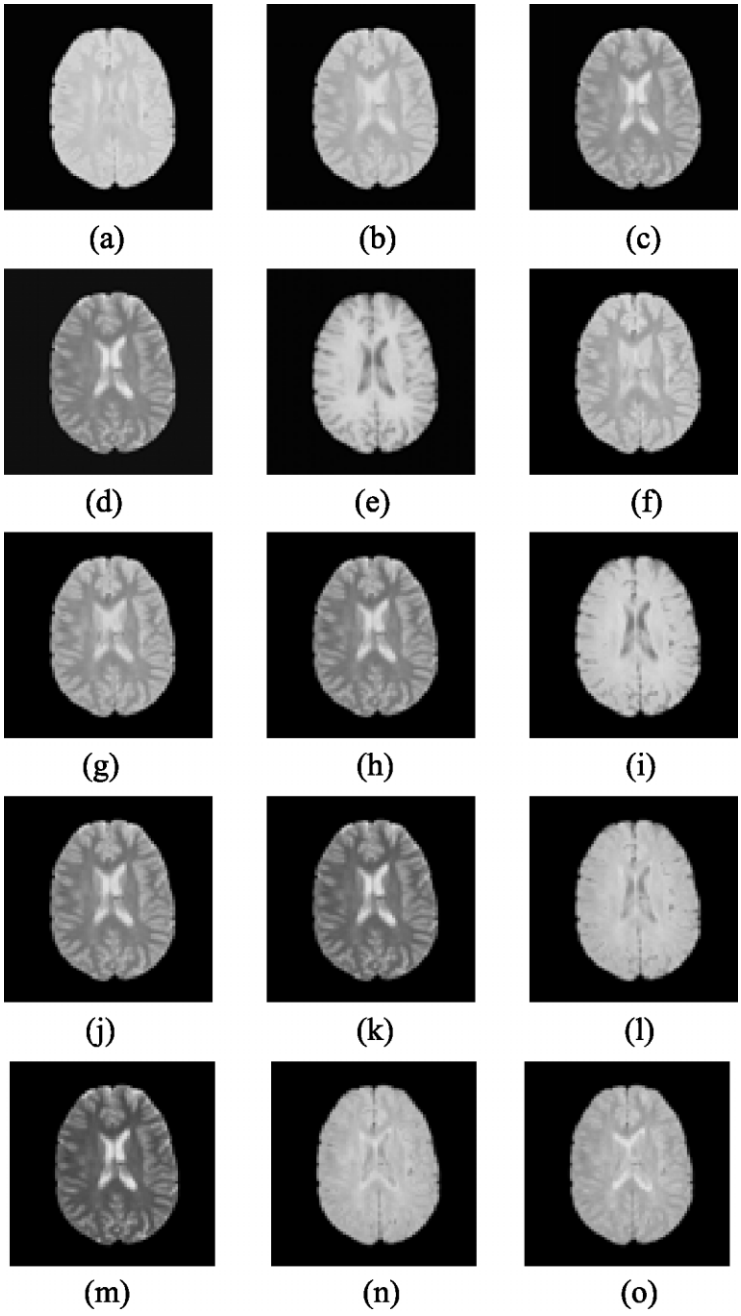

Fig. 9. New images generated by square root.

1.2. generate $\{B_iB_j\}_{i,j=1,i\neq j}^{l}$ = set of cross-correlated band images;
1.3. generate $\{\sqrt{B_i}\}_{i=1}^{l}$ = set of band images stretched out by the square-root;
1.4. form a new set of images which combines the original MR image sequence $\{B_i\}_{i=1}^{l}$ with images generated by (1),(2) and (3).

2. Apply OSP or SSC or OBC to the newly generated set obtained in (1.4) in step (1) to classify desired objects:
2.1. design a projector to eliminate undesired signatures;
$P_{\mathbf{U}}^{\perp}$ for OSP given by Eq. (3) or
$P_{\mathbf{U}}^{\perp}P_{\mathbf{M}}$ for SSC given by Eq. (10) or
$(\mathbf{d}^T\mathbf{d})^{-1}E_{\mathbf{dU}}$ for OBC with $E_{\mathbf{dU}}$ given by Eq. (12)
2.2. make use of the matched filter $MF_{\mathbf{d}}$ given by Eq. (6) to extract the desired signature $\mathbf{d}$.

5. Experimental results

A set of a brain MR image sequence was used to evaluate the performance of OSP and GOSP. It consists of MR images acquired from a patient with normal

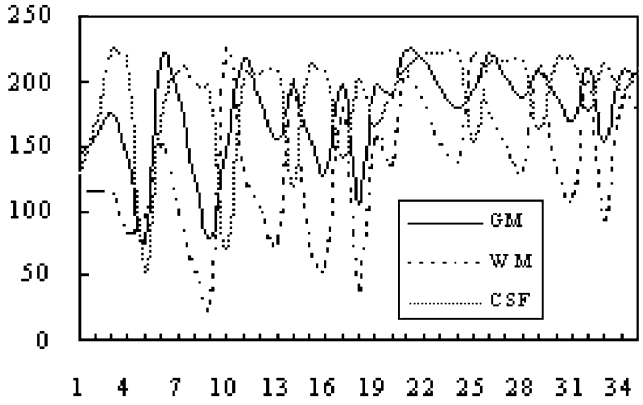

Fig. 10. Expanded spectra of WM, GM and CSF.

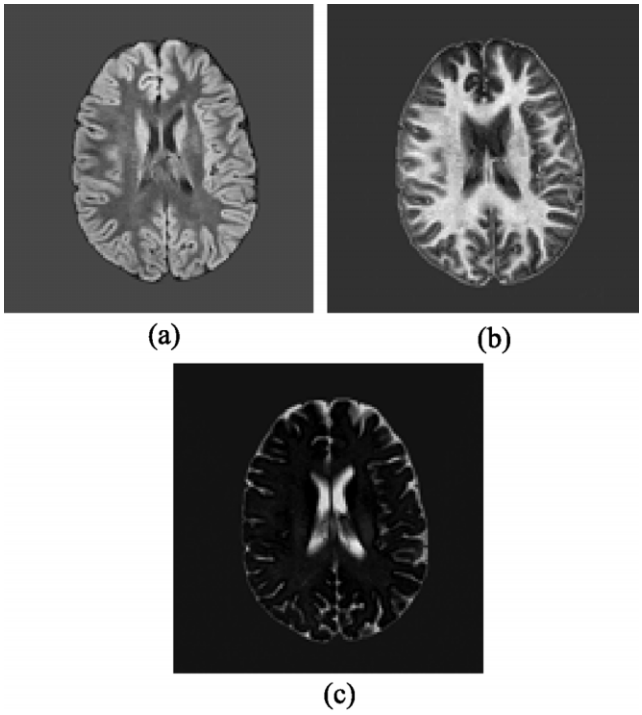

Fig. 11. Classification results of GOSP.

physiology shown in Fig. 1 using five spectral bands with 8-bit gray levels and size of 256 by 256 pixels. T1-weighted image is band 5 image which was acquired by the pulse sequence TR/TE = 2500/20 ms. T2-weighted images are bands 2, 3, 4 which were acquired by the pulse sequences TR/TE = 1500/55, TR/TE = 2500/75 and TR/TE = 2500/100 ms respectively. PD-weighted image is band 1 which was acquired by the pulse sequence TR/TE = 500/20 ms.

The spectral signatures of three cerebral tissues, gray matter (GM), white matter (WM) and cerebral spinal fluid (CSF) used for OSP and GOSP were extracted directly from the MR images and verified by experienced radiologists. They are shown in Fig. 2. Figs. 3–5 show the classification results of OSP, SSC and OBC based on

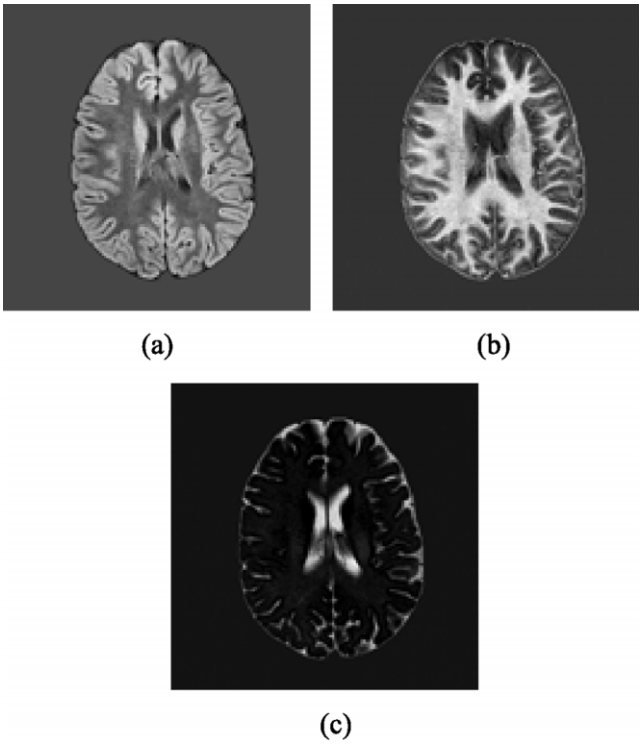

Fig. 12. Classification results of GSSC.

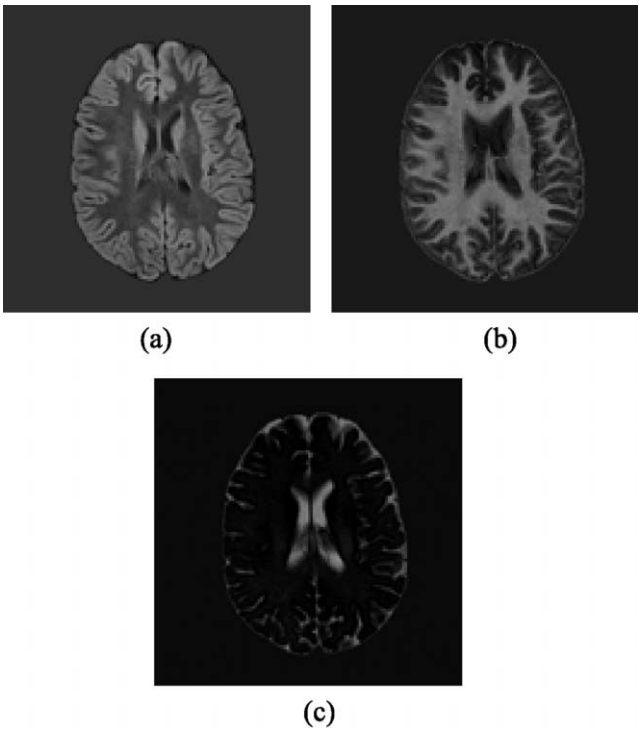

Fig. 13. Classification results of GOBC.

the five images in Fig. 1 where the images labeled by (a), (b) and (c) were generated respectively by using GM, WM and CSF as desired signatures **d** in the classifiers while the other two signatures were made up to

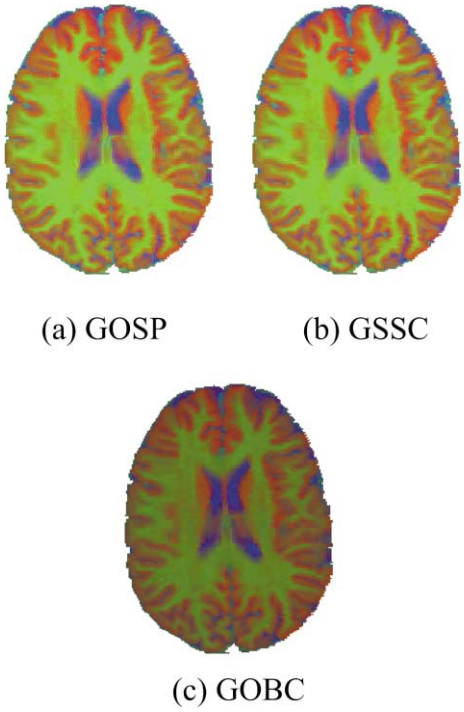

Fig. 14. RGB-colored classification results for GOSP, GSSC and GOBC.

form the undesired signature matrix **U**. As we can see, OSP-based classifiers performed well in classifying GM, WM and CSF and their results are very close. Nevertheless, it should be noted that according to computer simulations conducted in [23,32,33] SSC and OBC produced more accurate abundance fractions than did OSP. The reason that there is no appreciable difference among the images in Figs. 3–5 is because all the three OSP-based classifiers generate the same classification vector $\mathbf{d}^T P_U^{\perp}$ with different scaling constants. In particular, it has shown in [23,33] that OBC is equivalent to the maximum likelihood classifier provided the additive noise in the linear spectral mixture model described by Eq. (1) is Gaussian. When the images generated by OSP, SSC and OBC are all scaled to 256 gray levels for 8-bit computer display, these scaling constants are absorbed in the scaling process for computer display. So, from a display point of view, they all produce nearly the same results as shown in Figs. 3–5. Furthermore, by means of Figs. 3–5, we obtained RGB-colored classification results for OSP, SSC and OBC shown in Fig. 6 by assigning red color to GM-classified images [Figs. 3(a), 4(a) and 5(a)], green color to WM-classified images [Figs. 3(b), 4(b) and 5(b)] and CSF-classified images [Figs. 3(c), 4(c) and 5(c)]. The advantage of using color images for classification is that different degrees of target classification can be shown by different mixing colors. For example, 50% of red mixed with 50% of green results in yellow color. So, mixing colors may indicate that there are gray regions where the three tissues can be differentiated well from each other. This is an advantage of mixed pixel classification over the pure pixel classification where the former uses the abundance fractions to classify specific substances opposed to the latter which uses a binary decision for class-membership assignment. In addition, a mixing color can be also used for edge detection. We can see from these color images that OBC, i.e. maximum likelihood classifier produced a rather low contrast color image than did OSP and SSC.

In order to apply GOSP-based classifiers, a set of new 30 images was generated by DE. The images in Figs. 7–9 were generated by auto-correlation, cross-correlation and square-root respectively. Fig. 10 shows the expanded spectral signatures of WM, GM and CSF by combining five images in Fig. 1 with 30 images in Figs. 7–9. Using a total of 35 images in Fig. 1 plus Figs. 7–9, the classification results of GOSP, GSSC and GOBC are shown in Figs. 11–13. Like Figs. 3–5, the images labeled by (a), (b) and (c) are generated respectively by using GM, WM and CSF as desired signatures **d** in the classifiers while the other two signatures were made up to form the undesired signature matrix **U**. Compared Figs. 11–13 against those in Figs. 3–5, the GOSP-based classifiers improved OSP-based classifiers, specifically, noise and other unknown interferers have been significantly suppressed (e.g. WM classification) and the edges between GM, WM and CSF have been enhanced. A similar comment to the classification performance made for OSP, SSC and OBC also holds for GOSP, GSSC and GOBC. Using the same RGB assignment to that used for Fig. 6, the RGB-colored classification results for GOSP, GSSC and GOBC are shown in Fig. 14. Once again, the color image produced by GOBC has low contrast than did GOSP and GSSC.

6. Conclusion

Orthogonal subspace projection (OSP)-based approaches have been successfully applied to remotely sensed images in target detection and classification. This paper presents a new application of OSP in MR image classification. It views an MR image sequence as a multispectral image cube and models each pixel vector as a linear mixture of tissue substances resident in the MR pixel vector. Based on this linear mixture model several OSP-based classifiers can be derived for MR image classification. Unlike traditional image classification techniques which are carried out on a pure pixel basis, OSP-based classifiers are mixed pixel classification techniques. They use the linear mixture model to generate a fractional image for each object required for classification. The advantages of mixed pixel classification have been demonstrated in the experiments. Interestingly, OSP was shown to be equivalent to Soltanian-Zadeh et al.'s Euclidean distance-based discriminant analysis approach

with the constraint that the target vectors of interest are orthogonal [17]. OBC was also shown to be equivalent to the maximum likelihood classifier if the additive noise is Gaussian [33,34]. In order to further improve the OSP performance, a data dimensionality expansion procedure is introduced to extend the capability of OSP classifiers which results in a generalized OSP (GOSP). Experimental results show that OSP-based approaches have potential usefulness in MR image classification.

References

[1] Johnston B, Atkins MS, Mackiewich B, Anderson M. Segmentation of multiple sclerosis lesions in intensity corrected multispectral MRI. IEEE Transactions on Medical Imaging 1996;15(2):154–69.

[2] Atkins MS, Blair T, Mackiewich BT. Fully automatic segmentation of brain in MRI. IEEE Transactions on Medical Imaging 1998;17(1):98–107.

[3] Dhawan AP, Zavaljevski A, Sarwal A, Ball WS. A system for MR brain image segmentation. 18th Annual International Conference of the IEEE Engineering in Medicine and Biology Society, Amsterdam, 1996. p. 732–3.

[4] Verard L, Fadili J, Ruan S, Daniel Bloyet D. 3D MRI segmentation of brain structures. 18th Annual International Conference of the IEEE Engineering in Medicine and Biology Society, Amsterdam, 1996. p. 1081–2.

[5] Reddick WE, Glass JO, Cook EN, Elkin TD, Deaton RJ. Automated segmentation and classification of multispectral magnetic resonance images of brain using artificial neural networks. IEEE Transactions on Medical Imaging 1997;16(6):911–8.

[6] Alirezaie J, Jernigan ME, Nahmias C. Automatic segmentation of cerebral MR images using artificial neural networks. IEEE Transactions on Nuclear Science 1998;45(4):2174–82.

[7] Li JS, Chen RM, Huang YM. Medical image segmentation using mean field annealing network. IEEE International Conference on Image Processing 1997;2:855–8.

[8] Lin JS, Cheng KS, Mao CW. Multispectral magnetic resonance images segmentation using fuzzy Hopfield neural network. International Journal of Biomedical Computing 1996:205–14.

[9] Lin JS, Cheng KS, Mao CW. Modified Hopfield neural network with fuzzy c-means technique for multispectral MR image segmentation. IEEE International Conference on Image Processing 1996;1:327–30.

[10] Atkins MS, Mackiewich BT. Fully automatic segmentation of brain in MRI. IEEE Transactions on Medical Imaging 1998;17(1):98–107.

[11] Clark MC, Hall LC, Goldgof DB, Velthuizen R, Murtagh FR, Silbiger S. Automatic tumor segmentation using knowledge-based techniques. IEEE Transactions on Medical Imaging 1998;17(2):187–201.

[12] Windham JP, Abd-Allah MA, Reimann DA, Froehich JW, Haggar AM. Eigneimage filtering in MR imaging. J Computer Assisted Tomography 1998;12(1):1–9.

[13] Haggar AM, Windham JP, Reimann DA, Hearshen DC, Froehich JW. Eigneimage filtering in MR imaging: an application in the abnormal chest wall. Magnetic Resonance in Medicine 1989; 11:85–97.

[14] Soltanian-Zadeh H, Windham JP. Novel and general approach to linear filter design for contrast-to-noise ratio enhancement of magnetic resonance images with multiple interfering features in the scene. J Electronic Imaging 1992;1(2):171–82.

[15] Soltanian-Zadeh H, Windham JP, Peck DJ, Yagle AE. A comparative analysis of several transformations for enhancement and segmentation of magnetic resonance image scene sequences. IEEE Transactions on Medical Imaging 1992;11(3):302–16.

[16] Soltanian-Zadeh H, Saigal R, Haggar AM, Windham JP, Yagle AE, Hearshen DC. Optimization of MRI protocola and pulse sequence parameters for eigneimage filtering. IEEE Transactions on Medical Imaging 1994;13(1):161–75.

[17] Soltanian-Zadeh H, Windham JP, Peck DJ. Optimal linear transformation for MRI feature extraction. IEEE Transaction on Medical Imaging 1996;15(6):749–67.

[18] Harsanyi JC, Chang CI. Hyperspectral image classification and dimensionality reduction: an orthogonal subspace projection approach. IEEE Trans Geoscience and Remote Sensing 1994; 32(4):779–84.

[19] Miller JWV, Windham JP, Kwatra SC. Optimal filtering of radiographic image sequences using simultaneous diagonalization. IEEE Transactions on Medical Imaging 1984;MI-3:116–23.

[20] Miller JWV, Farison JB, Shin Y. Spatially Invariant Image Sequences. IEEE Transaction on Image Processing 1992;1(2):148–61.

[21] Du Q, Chang CI. A linear constrained distance-based discriminant analysis for hyperspectral image classification. Pattern Recognition 2001;34(2):361–73.

[22] Schwengredt RA. Remote sensing: Models and Methods for image processing, 2nd ed. New York: Academic Press, 1997. p. 470–1.

[23] Chang CI, Zhao XL, Althouse MLG, Pan JJ. Least squares orthogonal subspace approach to mixed pixel classification for hyperspectral images. IEEE Trans Geoscience and Remote Sensing 1998; 36(3):898–912.

[24] Chang CI, Sun TL, Althouse MLG. Unsupervised interference rejection approach to target detection and classification for hyperspectral imagery. Optical Engineering 1998;37(3):735–43.

[25] Chang CI, Brumbley C. A Kalman filtering approach to multispectral image classification and detection of change in signature abundance. IEEE Trans Geoscience and Remote Sensing 1999;37(1):257–68.

[26] Epp SS. Discrete mathematics with applications. 2nd ed. Brooks/Cole Publishing Company, 1995.

[27] Brumbley C. Kalman filtering and subspace approach to multispectral and hyperspectral image classification, PhD dissertation, Department of Electrical Engineering, University of Maryland Baltimore County, May 1998.

[28] Ren H, Chang CI. A generalized orthogonal subspace projection approach to unsupervised multispectral image classification. IEEE Trans on Geoscience and Remote Sensing 2000;38(6):2515–28.

[29] Adams JB, Smith MO. Spectral mixture modeling: a new analysis of rock and soil types at the Viking Lander 1 site. J Geophys Res 1986;91:8092–112.

[30] Shimabukuro YE, Smith JA. Least squares mixing models to generate fraction images derived from multispectral data. IEEE Trans Geosci Remote Sensing 1991;29(1):16–20.

[31] Adams JB, Smith MO, Gillespie AR. Image spectrocopy: interpretation based on spectralmixture analysis. In: Pieters CM, Englert PA, editors. Remote geochemical analysis: Elemental and mineralogical composition, Cambridge University Press, 1993. p. 145–66.

[32] Heinz D, Chang CI. Fully constrained least squares linear mixture analysis for material quantification in hyperspectral imagery. IEEE Trans on Geoscience Remote Sensing 2001;39(3):529–45.

[33] Chang CI. Further results on relationship between spectral unmixing and subspace projection. IEEE Trans Geoscience and Remote Sensing 1998;36(3):1030–2.

[34] Settle JJ. On the relationship between spectral unmixing and subspace projection. IEEE Trans on Geoscience Remote Sensing 1996;34(4):1045–6.

Chuin-Mu Wang received his BS degree in Electronic Engineering from National Taipei Institute of Technology and his MS degree in Information Engineering from Tatung University of Taiwan in 1984 and 1990, respectively. From 1984 to 1990, he was a System Programmer on an IBM mainframe system and from 1990 to 1992, he was a Marketing Engineer on computer products at Tatung Company. Since 1992, he has been a lecturer at the Chinyi Institute of Technology. His research interests include database, multispectral image processing, and medical imaging.

Sheng-Chih Yang received his BS degree in Electronic Engineering from National Chin-Yi Institute of Technology, Taiwan in 1987 and his MS degree in Computer and Information Science from Knowledge System Institute, Illinois, USA in 1996. He is now working on a PhD degree at the department of Electrical Engineering, National Cheng-Kung University, Taiwan. From 1992 to 1995, he worked as a Teaching Assistant at the Department of Electronic Engineering, National Chin-Yi Institute of Technology. Since 1995, he has been a Lecturer of National Chin-Yi Institute of Technology. His research interests include digital image processing and biomedical image processing.

Pau-Choo Chung received BS and MS degrees in Electrical Engineering from National Cheng Kung University, Tainan, Taiwan in 1981 and 1983, respectively, and a PhD degree in Electrical Engineering from Texas Tech University, Lubbock in 1991. From 1983 to 1986, she was with the Chung Shan Institute of Science and Technology, Taiwan. Since 1991, she has been with Department of Electrical Engineering, National Cheng Kung University, where she is currently a Full Professor. Her current research includes neural networks, and their applications to medical image processing, medical image analysis, telemedicine, and video image analysis.

Chein-I Chang received a BS degree from Soochow University, Taipei, Taiwan in 1973, an MS degree from the Institute of Mathematics at National Tsing Hua University, Hsinchu, Taiwan in 1975 and an MA degree from Stony Brook in 1977, all in Mathematics. He also received his MS, MSEE degrees from the University of Illinois at Urbana-Champaign, in 1982 and a PhD degree in Electrical Engineering from the University of Maryland, College Park in 1987. Dr Chang has been with the University of Maryland Baltimore County (UMBC) since 1987, first as Visiting Assistant Professor from January 1987 to August 1987, Assistant Professor from 1987 to 1993, and Associate Professor from 1993–2001 and Professor in the Department of Computer Science and Electrical Engineering in 2001. He was a Visiting Research Specialist in the Institute of Information Engineering at the National Cheng Kung University, Tainan, Taiwan from 1994 to 1995. He has a patent on automatic pattern recognition and several pending patents on image processing techniques for hyperspectral imaging and detection of microcalcifications. He is currently on the editorial board of *Journal of High Speed Networks* and is the Guest Editor of a special issue of that journal on Telemedicine and Applications. His research interests include automatic target recognition, multispectral/hyperspectral image processing, medical imaging, information theory and coding, signal detection and estimation, neural networks. Dr Chang is a senior member of IEEE and a member of SPIE, INNS, Phi Kappa Phi and Eta Kappa Nu.

Chien-Shun Lo received BS and MS degrees in Information Engineering and Computer Science from Feng-Chia University, Taiwan in 1992 and 1994, respectively. He is now working on a PhD degree at the institute of Electrical Engineering, National Cheng-Kung University, Taiwan. He is also a Research Assistant at the Department of Radiology, Taichung Veterans General Hospital, Taiwan. His current research interests are image processing, medical image processing and analysis, computer-aided diagnostic system.

Chi-Chang Chen received an MD degree in Medical Science from China Medical College, Taiwan in 1981. From 1983 to 1988 he was a Resident at Department of Radiology of Taichung Veterans General Hospital. He became a Visiting Staff from 1988 to 1995. Since 1995, he has serviced as Director of the Department of Neuro of Radiology of Taichung Veterans General Hospital. His current research interests are CT, MRI, and functional MRI.

Chin-Wen Yang received a BS degree in Information Engineering sciences from Feng-Chia University, Taiwan in 1987, an MS degree in Information Engineering from National Cheng Kung University in 1989, and a PhD degree in Electrical Engineering from National Cheng Kung University, Taiwan, Republic of China in 1996. He is currently a Technique Chief in the Computer and Communication Center, Taichung Veterans General Hospital, Taiwan. His research interests include image processing, biomedical image processing, and computer network.

Chia-Hsien Wen was born in Taipei, Taiwan, on 2 August 1954. He received his BS degree in Computer Sciences from TamgKang University, Taiwan in 1976, and an MS degree in Applied Mathematics and the PhD degree in computer science from National Tsing-Hua University, Taiwan in 1978 and 1994, respectively. From 1979 to 1982, he worked at Taipei Veterans General Hospital, Taiwan, as a System Analyst. Since 1982, he has been the Director of Computer and Communication Center, Taichung Veterans General Hospital, Taiwan. His research interests include image processing, biomedical image processing, and hospital information systems.